

Article

An Adaptive Control Scheme Based on Non-Interference Nonlinearity Approximation for a Class of Nonlinear Cascaded Systems and Its Application to Flexible Joint Manipulators

Zhangxing Liu, Hongzhe Jin *  and Jie Zhao

School of Mechatronics Engineering, Harbin Institute of Technology, Harbin 150001, China; liuzhangxinghit@163.com (Z.L.); jzhao@hit.edu.cn (J.Z.)

* Correspondence: hongzhejin@hit.edu.cn

Abstract: Control design for the nonlinear cascaded system is challenging due to its complicated system dynamics and system uncertainty, both of which can be considered some kind of system nonlinearity. In this paper, we propose a novel nonlinearity approximation scheme with a simplified structure, where the system nonlinearity is approximated by a steady component and an alternating component using only local tracking errors. The nonlinearity of each subsystem is estimated independently. On this basis, a model-free adaptive control for a class of nonlinear cascaded systems is proposed. A squared-error correction procedure is introduced to regulate the weight coefficients of the approximation components, which makes the whole adaptive system stable even with the unmodeled uncertainties. The effectiveness of the proposed controller is validated on a flexible joint system through numerical simulations and experiments. Simulation and experimental results show that the proposed controller can achieve better control performance than the radial basis function network control. Due to its simplicity and robustness, this method is suitable for engineering applications.

Keywords: model-free adaptive control; nonlinearity approximation; cascaded system; flexible joint



Citation: Liu, Z.; Jin, H.; Zhao, J. An Adaptive Control Scheme Based on Non-Interference Nonlinearity Approximation for a Class of Nonlinear Cascaded Systems and Its Application to Flexible Joint Manipulators. *Sensors* **2024**, *24*, 3178. <https://doi.org/10.3390/s24103178>

Academic Editors: Yuanlong Xie, Shiqi Zheng, Zhaozheng Hu and Shuting Wang

Received: 4 February 2024

Revised: 12 May 2024

Accepted: 13 May 2024

Published: 16 May 2024



Copyright: © 2024 by the authors. Licensee MDPI, Basel, Switzerland. This article is an open access article distributed under the terms and conditions of the Creative Commons Attribution (CC BY) license (<https://creativecommons.org/licenses/by/4.0/>).

1. Introduction

The control problem of nonlinear cascaded systems commonly exists in engineering. Mechanical joints in robot manipulators are driven by motor currents [1–3]. The path tracking control of mobile robots is realized by adjusting wheel velocities [4–7]. Gyroscopic precession can be integrated into one-wheeled robots for steering control [8]. Flight dynamics in unmanned aerial vehicles (UAVs) can be stabilized through attitude adjustment [9–12]. Although these systems vary in physical assumptions, all of them can be modeled as nonlinear systems with a cascaded structure. The control design for such systems is challenging due to complicated system nonlinearity and uncertainty.

Disturbance rejection is a common approach to addressing the effects of unknown system nonlinearity and uncertainty. References [13,14] apply H-infinity optimal control for the linear system to suppress the effects of unknown disturbances. However, for systems with strong uncertainties, linear H-infinity control may lead to conservative performance. Hence, some researchers develop H-infinity controllers based on nonlinear system models [15–17]. Compared to the linear version, nonlinear H-infinity control allows for greater system nonlinearity under fine-tuning conditions and can delay control degradation and instability risks [17]. However, solving for nonlinear H-infinity controllers is usually complex and time-consuming [15,17,18]. In addition, invariant ellipsoid techniques are also introduced to optimize the robustness of control systems to unknown disturbances [19]. The invariant ellipsoid method simplifies the optimal controller to finding the smallest invariant ellipsoid of the closed-loop dynamic system [20]. A typical way is to apply the invariant ellipsoid method to suppress persistent disturbances through state-feedback control via LMI techniques [21–23]. It needs to quantitatively evaluate the effects of disturbances

on the system output; thus, accurate system information is required. Other methods, such as the generalized fractional equation [24], are also introduced to model complex, uncertain systems.

Obtaining optimal control solutions for nonlinear systems with complex uncertainties is often challenging. Hence, researchers have proposed to combine the aforementioned disturbance rejection methods with nonlinearity estimation approaches that are free from system models, such as artificial neural networks (ANN) [25,26], fuzzy networks [27], and disturbance observers [18,28,29].

Artificial intelligence networks, such as fuzzy systems and neural networks, are commonly used for nonlinearity approximation [30–37]. In [31], a fuzzy approximation-based adaptive backstepping controller was developed to assist in the movement of an upper-limb exoskeleton robot. References [33–35] present observer-based fuzzy neural-network output feedback control algorithms for underactuated nonlinear systems. These studies combine the adaptive backstepping technique with artificially intelligent networks to achieve a high-performance approximation-based controller. Reference [38] proposes a reinforcement learning-based method to ensure asymptotic tracking control of continuous-time systems. However, the application of these approaches is hindered by complex control objects with a high degree of freedom (DOF), structural uncertainty, and system nonlinearity [36]. For artificial intelligence networks with complex topological structures, the learning process degrades the transient performance of the system and requires high calculation efficiency. For real-time control systems, their high computational cost is an inevitable challenge. References [32,36,37] stated that these factors impede the development of intelligence networks-based adaptive control, especially in real-time control applications.

High-gain disturbance observer (HGDOB) and sliding mode control (SMC) are also effective methods to deal with systems with parametric uncertainties and unmodeled nonlinearities. In [39], a HGDOB is designed to estimate the system disturbance caused by friction, load force, and the parameter disturbance for electro-hydraulic systems. However, the high gain observer is sensitive to measurement noise and delayed outputs [40]. To solve this problem, Reference [41] designed time-varying gains relying on the generalization of the Halanay-type inequalities. Reference [42] tried to lower the observer gain by introducing artificial delays and Taylor's series. Similarly, the SMC is limited by chattering and peak phenomena in control signals [43]. In [44], a radial basis function neural network (RBFNN)-based soft computing strategy is applied to avoid the high switching gain that leads to chattering amplification. In [45], an adaptive sliding mode control method (ASMC) for robot manipulators is introduced. It utilizes the Taylor expansion to achieve a less conservative sign-function gain that enables chattering attenuation. The above approaches reduce chattering by applying extra-complicated policies. An interesting work is presented in [46] that presents a finite-time SMC (FT-SMC) and suppresses the peak phenomenon and chattering with an asymptotically convergent differentiator.

As can be seen from the previous discussion, in order to deal with unknown disturbances while avoiding problems caused by high control gains, controllers tend to become more and more complex and bloated. It is particularly unfriendly for engineering applications. Therefore, a simplified controller that is robust to unknown system nonlinearities and possesses mild control input is valuable for engineering applications.

Hence, this study aims to provide a simplified adaptive controller for a class of nonlinear cascaded systems. We first propose a so-called non-interference nonlinearity approximation (NINA) technique. It is based on the following system theory: For stable closed-loop systems, a bounded and continuous system nonlinearity can always be decomposed into steady and alternating components [47]. Furthermore, the output errors incorporated information relating to the system nonlinearity. Therefore, the unknown system nonlinearity can be modeled as a hierarchical form of a steady component and an alternating component. In addition, each nonlinearity can be approximated independently, using only local tracking errors. Thus, the proposed scheme is called non-interference nonlinearity approximation. Due to the simplified and decoupled approximation structure, the

computational complexity of NINA is significantly reduced. Based on NINA, a model-free adaptive control is proposed. It is convenient for engineering applications because it avoids the fussy process of system modeling and parameter identification. In addition, it is also robust to external disturbance and parameter perturbation due to accurate nonlinearity approximation and compensation, which are verified by numerical simulations and experiments. Finally, its control inputs are milder than those of SMC and HGDOB-based control.

In summary, the contributions of this work are as follows:

- (1) A novel NINA scheme that has a simplified hierarchical structure is proposed. Based on only local tracking errors, the NINA technique can approximate the unknown system nonlinearity regardless of its internal complexity. Saturation functions with adjustable shaping factors help balance fast convergence against measurement noise, thereby providing a mild control input.
- (2) A model-free adaptive control based on the NINA technique is proposed. Its uniformly ultimate boundedness (UUB) is proven by the Lyapunov theory. The effectiveness and robustness have been validated by simulations and experiments on a flexible-joint manipulator system.
- (3) Compared with the intelligence network-based control, the proposed method possesses a simplified structure and requires less computational costs. Compared with the SMC, the proposed method can perform fast trajectory tracking with mild control inputs. Hence, it is convenient for engineering applications.

Reference [48] introduces an adaptive weighted saturation function to suppress system uncertainty in a stabilization problem. The approach was applied to flexible manipulator control by [49,50]. Different from previous work, this paper approximates the nonlinearity of the closed-loop system using trajectory tracking errors instead of relying on system states. Furthermore, a hierarchical approximation structure is introduced in this paper. The steady component aims to achieve fast tracking for the major part of the nonlinearity, while the alternating component is designed to supplementarily track its high-frequency fluctuations. In addition, this paper conducted an elaborate theoretical analysis that not only proves the effectiveness of the proposed approximation method but also provided the upper bound of the approximation error. The convergence of the weighted parameters was also analyzed. Hence, this work can be viewed as an extension of the approach in [48] to some degree.

The remainder of this paper is organized as follows: Section 2 formulates the dynamic model for a class of nonlinear cascaded systems. Section 3 presents a decoupled control framework. Section 4 describes the NINA technique. On this basis, Section 5 proposes NINA-based adaptive control. Numerical simulations and experiments on the flexible joint system are presented in Sections 6 and 7, respectively. Conclusions are provided in Section 8.

2. Preliminaries

Mathematical Description of the Generalized Dynamics

First, we consider a class of nonlinear cascaded systems with n-DOF whose dynamics are given by:

$$\begin{bmatrix} m_\alpha(\alpha, \beta) & m_{\alpha\beta}(\alpha, \beta) \\ m_{\beta\alpha}(\alpha, \beta) & m_\beta(\alpha, \beta) \end{bmatrix} \begin{bmatrix} \ddot{\alpha} \\ \ddot{\beta} \end{bmatrix} + \begin{bmatrix} n_\alpha(\alpha, \dot{\alpha}, \beta, \dot{\beta}) \\ n_\beta(\alpha, \dot{\alpha}, \beta, \dot{\beta}) \end{bmatrix} = \begin{bmatrix} 0 \\ \tau_\beta \end{bmatrix} \quad (1)$$

where $\alpha, \beta \in \mathbb{R}^n$ represent the coordinates. $m_\alpha, m_{\alpha\beta}, m_{\beta\alpha}, m_\beta \in \mathbb{R}^{n \times n}$ form the system inertia matrix. $n_\alpha, n_\beta \in \mathbb{R}^n$, represent the system nonlinearity that captures centrifugal and Coriolis forces, viscous and frictions, gravitation, unmodeled system dynamics, and external disturbances. $\tau_\beta \in \mathbb{R}^n$ represents the control inputs. The first and second rows in

(1) represent the unactuated and actuated subsystems, respectively. For the convenience of distinguishing, they are denoted as the α -system and β -system.

For cascaded systems [1–12], the nonlinearity of the α -system n_α usually contains a dynamic coupling term that coordinates the behavior of the actuated and unactuated subsystems. Hence, n_α can be modeled as the combination of a known dynamic coupling term and a residual term, i.e.,

$$n_\alpha(\alpha, \dot{\alpha}, \beta, \dot{\beta}) = \delta_\alpha(\alpha, \dot{\alpha}, \beta, \dot{\beta}) - u_\alpha(\alpha, \dot{\alpha}, \beta, \dot{\beta}) \quad (2)$$

where u_α is the known dynamic coupling term and δ_α is the unmolded system nonlinearity.

Substituting (2) into (1), the dynamic model can be represented as

$$\begin{bmatrix} m_\alpha(\alpha, \beta) & m_{\alpha\beta}(\alpha, \beta) \\ m_{\beta\alpha}(\alpha, \beta) & m_\beta(\alpha, \beta) \end{bmatrix} \begin{bmatrix} \ddot{\alpha} \\ \ddot{\beta} \end{bmatrix} + \begin{bmatrix} \delta_\alpha(\alpha, \dot{\alpha}, \beta, \dot{\beta}) \\ n_\beta(\alpha, \dot{\alpha}, \beta, \dot{\beta}) \end{bmatrix} = \begin{bmatrix} u_\alpha(\alpha, \dot{\alpha}, \beta, \dot{\beta}) \\ \tau_\beta \end{bmatrix} \quad (3)$$

where the behavior of the α -system is indirectly regulated by the dynamic coupling term u_α . Given the states of the α -system, the value of u_α depends on the states of the β -system. Therefore, the control objective is to perform trajectory tracking control of the α -system by regulating the behavior of the β system.

Assumption 1. Let $x = (\alpha, \dot{\alpha})$, $y = (\beta, \dot{\beta})$. For any given $y_1, y_2 \in \mathbb{R}^n$, u_α satisfies the following Lipschitz condition:

$$\|u_\alpha(x, y_2) - u_\alpha(x, y_1)\| \leq \gamma \|y_2 - y_1\|, \quad (4)$$

where $\gamma > 0$ is a finite constant.

Assumption 2. Let S_1 , S_2 , and S_3 be the ranges of x , y , and u_α , respectively. We have $u_\alpha : (S_1 \times S_2) \rightarrow S_3$. Given $x \in S_1$, for any desired $u_\alpha \in S_3$, there exists $y_r \in S_2$ satisfying the following inverse mapping:

$$u_\alpha^{-1} : (u_{\alpha r} \times x) \rightarrow y_r, \quad (5)$$

where $u_{\alpha r}$ is the desired value of u_α , and y_r is the desired value of y . This assumption is summarized from real systems [1–12].

Remark 1. Assumptions 1 and 2 guarantee the maneuverability of the α -system. If we take $u_\alpha \in S_3$ as the virtual control and using (4) and (5), the error between $u_{\alpha r}$ and u_α is bounded by

$$\|u_\alpha(x, y_r) - u_\alpha(x, y)\| \leq \gamma \|y - y_r\|. \quad (6)$$

We have $u_\alpha(x, y) \rightarrow u_\alpha(x, y_r)$ as $y \rightarrow y_r$. It indicates that the α -system can be indirectly regulated by the β -system via the dynamic coupling term u_α .

Remark 2. Equations (1) and (2) with assumptions 1 and 2 represent a class of nonlinear cascaded systems where the unactuated subsystems are indirectly regulated by the behaviors of the actuated subsystems through dynamic coupling. Some examples are provided as follows: For the flexible joint manipulator, the flexibility torque connects the dynamic behavior of the load and motor sides [3]. The gyro moment is used to maintain the lateral balance of the gyroscopic pendulum robot [7]. Dynamic coupling between attitude regulation torque and thrust force is widely utilized for the path tracking control of UAVs [9–12]. In the above examples, flexibility torque, the gyro moment, and aerodynamics can be viewed as the known dynamic coupling terms that can be used for controller design.

3. Decoupled Control Framework

Considering system (1), there are two types of dynamic coupling: first, the dynamic coupling between the actuated and unactuated subsystems; and second, the dynamic coupling between different degrees of freedom (DOFs). To address the problem mentioned

above, a decoupled control framework is proposed in this paper, as shown in Figure 1. To deal with the dynamic coupling between the actuated and unactuated subsystems, we introduce a cascaded control framework where an α -controller is placed in the outer layer to stabilize the unactuated subsystem and a β -controller is positioned in the inner layer to regulate the actuated subsystem. The two sub-controllers are linked through the inverse mapping of the dynamic coupling term Γ_α . In addition, the dynamic coupling between different DOFs is considered to be an unknown disturbance and is compensated by the proposed NINA technique presented in the next section.

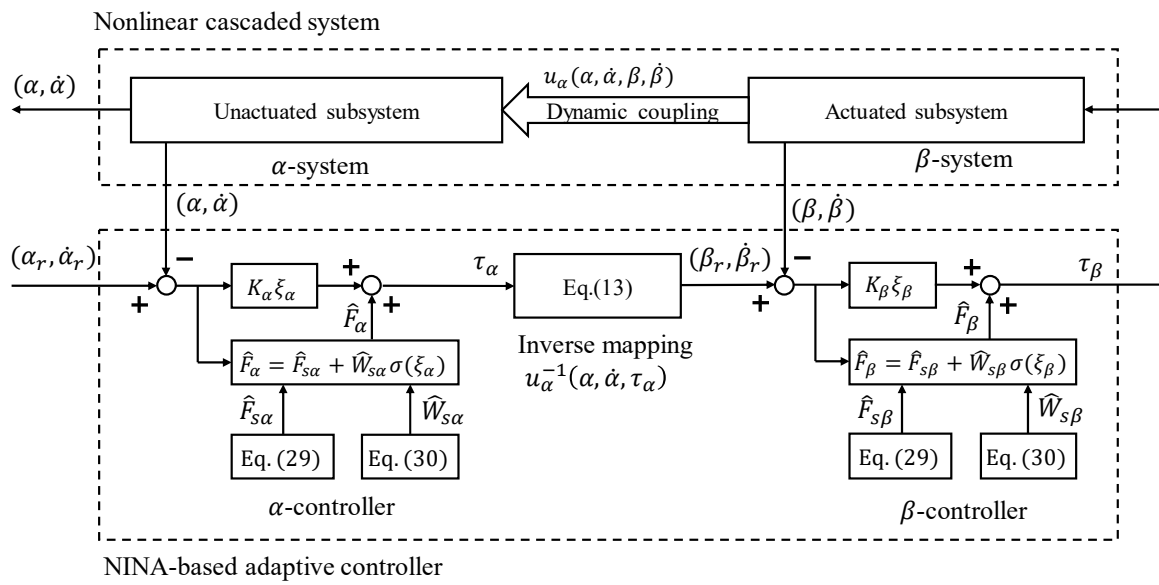


Figure 1. Decoupled cascaded control framework.

The control framework is derived below. Let $\alpha_r(t)$ and $\beta_r(t)$ be the reference trajectory of the α - and β -systems, which are assumed to be bounded and to have finite first- and second-order time derivatives. Let $e_\alpha = \alpha_r - \alpha$ and $e_\beta = \beta_r - \beta$ be the position tracking errors. Then, the following synthetic tracking errors are introduced:

$$\begin{aligned}\tilde{\zeta}_\alpha &= \Lambda_\alpha e_\alpha + \dot{e}_\alpha \\ \tilde{\zeta}_\beta &= \Lambda_\beta e_\beta + \dot{e}_\beta\end{aligned}\quad (7)$$

where $\Lambda_\alpha, \Lambda_\beta > 0$ are diagonal positive gain matrices. Substituting (7) into model (3) and applying $\tau_\alpha = u_{\alpha r}$ as the virtual control, the error dynamics can be expressed as

$$\begin{bmatrix} m_\alpha(\alpha, \beta) & m_{\alpha\beta}(\alpha, \beta) \\ m_{\beta\alpha}(\alpha, \beta) & m_\beta(\alpha, \beta) \end{bmatrix} \begin{bmatrix} \dot{\tilde{\zeta}}_\alpha \\ \dot{\tilde{\zeta}}_\beta \end{bmatrix} = \begin{bmatrix} m_\alpha(\alpha, \beta) & m_{\alpha\beta}(\alpha, \beta) \\ m_{\beta\alpha}(\alpha, \beta) & m_\beta(\alpha, \beta) \end{bmatrix} \begin{bmatrix} \Lambda_\alpha \dot{e}_\alpha + \ddot{\alpha}_r \\ \Lambda_\beta \dot{e}_\beta + \ddot{\beta}_r \end{bmatrix} + \begin{bmatrix} v_\alpha - \tau_\alpha \\ v_\beta - \tau_\beta \end{bmatrix}, \quad (8)$$

where $v_\alpha = \delta_\alpha + \tilde{u}_\alpha$ represents a lumped nonlinearity. $\tilde{u}_\alpha = u_{\alpha r} - u_\alpha$ is the distortion between the desired control input and its actual value. Such a distortion is mainly caused by state tracking errors, parameter perturbations, and the model uncertainty of u_α .

Let us analyze (8) by choosing the following Lyapunov function:

$$V_1 = \frac{1}{2} \tilde{\zeta}^T M \tilde{\zeta}, \quad (9)$$

with

$$\tilde{\zeta} = \begin{bmatrix} \tilde{\zeta}_\alpha \\ \tilde{\zeta}_\beta \end{bmatrix}, M = \begin{bmatrix} m_\alpha(\alpha, \beta) & m_{\alpha\beta}(\alpha, \beta) \\ m_{\beta\alpha}(\alpha, \beta) & m_\beta(\alpha, \beta) \end{bmatrix}.$$

Considering the time derivative of (9) and substituting (8), we obtain

$$\dot{V}_1 = \zeta^T (F - \tau), \quad (10)$$

with

$$\tau = \begin{bmatrix} \tau_\alpha \\ \tau_\beta \end{bmatrix},$$

$$F = \begin{bmatrix} F_\alpha \\ F_\beta \end{bmatrix} = \frac{1}{2} \begin{bmatrix} \dot{m}_\alpha(\alpha, \beta) & \dot{m}_{\alpha\beta}(\alpha, \beta) \\ \dot{m}_{\beta\alpha}(\alpha, \beta) & \dot{m}_\beta(\alpha, \beta) \end{bmatrix} \begin{bmatrix} \zeta_\alpha \\ \zeta_\beta \end{bmatrix} + \begin{bmatrix} m_\alpha(\alpha, \beta) & m_{\alpha\beta}(\alpha, \beta) \\ m_{\beta\alpha}(\alpha, \beta) & m_\beta(\alpha, \beta) \end{bmatrix} \begin{bmatrix} \Lambda_\alpha \dot{e}_\alpha + \ddot{\alpha}_r \\ \Lambda_\beta \dot{e}_\beta + \ddot{\beta}_r \end{bmatrix} + \begin{bmatrix} v_\alpha \\ n_\beta \end{bmatrix} \quad (11)$$

where F is an integrated system nonlinearity. Considering F as an unknown disturbance and compensating via nonlinearity estimation, a simplified control law can then be designed as

$$\tau = K\zeta + \hat{F}, \quad (12)$$

where K is a positive, definite diagonal gain matrix. \hat{F} is the estimation of F applied for nonlinearity compensation.

Substituting (12) into (10), \dot{V}_1 becomes

$$\dot{V}_1 = -\zeta^T K \zeta + \zeta^T (F - \hat{F}). \quad (13)$$

Ideally, if $\hat{F} = F$, ζ is asymptotically convergent to zero. If $\tilde{F} = F - \hat{F}$ is bounded, ζ will be ultimately bounded. It can be seen that the stability of the closed-loop system is determined by the nonlinearity approximation process. In the next section, a simplified NINA technique is proposed for the nonlinearity approximation.

Remark 3. As shown in Figure 1, the reference of the α -system $(\alpha_r, \dot{\alpha}_r)$ is given by users, while the reference of the β -system $(\beta_r, \dot{\beta}_r)$ is generated to guide the tracking of the virtual control $u_\alpha \rightarrow u_{\alpha r} = \tau_\alpha$.

Given the states of the α -system $(\alpha, \dot{\alpha})$ and the desired value of virtual control, $u_{\alpha r}$, we have

$$u_\alpha(\alpha, \dot{\alpha}, \beta, \dot{\beta}) \rightarrow u_{\alpha r}(\alpha, \dot{\alpha}, \beta_r, \dot{\beta}_r) \text{ as } (\beta, \dot{\beta}) \rightarrow (\beta_r, \dot{\beta}_r). \quad (14)$$

Hence, $(\beta_r, \dot{\beta}_r)$ can be obtained by solving the inverse mapping of $u_\alpha(\alpha, \dot{\alpha}, \beta_r, \dot{\beta}_r)$ with respect to $(\beta_r, \dot{\beta}_r)$, i.e.,

$$(\beta_r, \dot{\beta}_r) = u_\alpha^{-1}(\alpha, \dot{\alpha}, u_{\alpha r}). \quad (15)$$

An example of such inverse mapping about the elastic torque of the flexible joint manipulator is given in Equation (51).

4. Principles of NINA

In this section, a simplified nonlinearity approximation scheme is presented. The nonlinearity of each subsystem can be estimated independently by simply utilizing the local tracking error.

Declaration 1. Considering the nonlinearity approximation by each subsystem, we adopt the following symbolic notation: for a vector V or a diagonal matrix V , the j -th element is marked by V_j , where $j = 1, 2, \dots, 2n$.

Let F_j represents the system nonlinearity and is assumed to be a bounded continuous time function. In real-world applications, most of the plants are controlled by digital controllers. Therefore, F_j can be viewed as a piecewise time-varying function within successive control cycles. Mathematically, such a piecewise time-varying function can

always be expressed as the synthetic form of steady and alternating components [47]. Hence, the system nonlinearity can be modeled in the time-domain as

$$F_j(t) \equiv F_{sj} + \Delta_j(t), (t_I \leq t \leq t_I + \mu T_c) \quad (16)$$

where $\mu > 1$ is a positive integer. t_I is the initial moment, and T_c is the control cycle. F_{sj} and Δ_j denote a bounded steady component and a bounded alternating component, respectively.

In addition, for closed-loop control systems, the tracking error reflects the combined effect of system nonlinearities. Therefore, we introduce the following structure to approximate system nonlinearities with the synthetic tracking error ξ_j :

$$F_{Aj}(\xi_j) = F_{sj} + W_{sj}\sigma(\xi_j), (|\Delta_j| < W_{sj} < \infty), \quad (17)$$

where F_{Aj} is the approximation of F_j . F_{sj} is the steady component in (16), and $W_{sj}\sigma(\xi_j)$ is introduced to approximate the alternating component Δ_j , where W_{sj} is a dynamically adjusted weight coefficient and $\sigma(\xi_j)$ is a saturation function expressed as

$$\sigma(\xi_j) = \xi_j / (\vartheta_{sj} + |\xi_j|), (0 < \vartheta_{sj} < \infty), \quad (18)$$

where ϑ_{sj} is a shaping factor. When $\vartheta_{sj} \rightarrow 0$, $\sigma(\xi_j)$ acts as a signed switching function that is highly sensitive to the variation of ξ_j around zero. By contrast, when $\vartheta_{sj} \rightarrow \infty$, $\sigma(\xi_j)$ tends to zero and becomes insensitive to the changes of ξ_j . Compared with the linear or polynomial approximation, the introduced saturation function enables a wide range of sensitivity adjustment w.r.t. ξ_j via only one parameter. It is more convenient and adaptable.

From (16) and (17), the approximation error between $F_j(t)$ and F_{Aj} can be calculated as

$$E(\Delta_j, \xi_j) = F_j(t) - F_{Aj}(\xi_j) = \Delta_j(t) - W_{sj}\sigma(\xi_j). \quad (19)$$

Theorem 1. For a bounded continuous nonlinearity $F_j(t)$, there exist optimized parameters F_{sj} , W_{sj} , and ϑ_{sj} for the approximation structure (17), (18) that satisfy the identity $E(\Delta_j, \xi_j) = 0$ and the synthetic tracking error is ultimately bounded by

$$|\xi_j| \leq \vartheta_{sj}(|\Delta_j/W_{sj}|) / [1 + |\Delta_j/W_{sj}|], \quad (20)$$

where $|\xi_j| \rightarrow 0$, as $\vartheta_{sj} \rightarrow 0$ and $W_{sj} > |\Delta_j|$. It illustrates that the proposed structure can effectively approximate the system nonlinearity while maintaining a small synthetic tracking error.

Proof . Let $\hat{F}_j(t) = F_{Aj}(\xi_j)$ and substitute (19) into (13). The first derivative of the Lyapunov function in (13) becomes

$$\dot{V}_1 = -\sum_j K_j \xi_j^2 + \sum_j E(\Delta_j, \xi_j) \xi_j, \quad (21)$$

where $-K_j \xi_j^2 \leq 0$. The property of $E(\Delta_j, \xi_j) \xi_j$ is discussed below.

Step 1: The second derivatives of $E(\Delta_j, \xi_j) \xi_j$ with respect to ξ_j is presented as

$$\frac{\partial^2 E(\Delta_j, \xi_j) \xi_j}{\partial^2 \xi_j} = 2W_{sj}(\sigma(\xi_j) - 1)\sigma'(\xi_j), \quad (22)$$

where $\sigma'(\xi_j)$ is the first derivatives of $\sigma(\xi_j)$ with respect to ξ_j . It can be verified segmentally that $\frac{\partial^2 E(\Delta_j, \xi_j) \xi_j}{\partial^2 \xi_j} < 0$ for any $\xi_j \in R$ and $W_{sj} > 0$. Hence, $E(\Delta_j, \xi_j) \xi_j$ is an open downward convex function with respect to ξ_j . This can be further verified by the profile diagram shown in Figure 2.

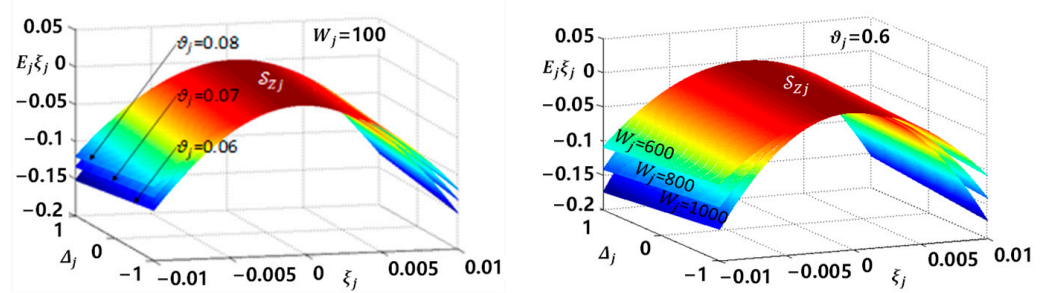


Figure 2. Changes in the profile of $E_j(\Delta_j, \zeta_j)\zeta_j$ caused by parameter drifts.

Step 2: Given that $E(\Delta_j, \zeta_j)\zeta_j$ is an open downward convex function with respect to ζ_j , its sign will vary around the nonzero solution $\zeta_j = \zeta_z(\Delta_j)$ of equation $E(\Delta_j, \zeta_j)\zeta_j = 0$. With (19), the value of $\zeta_z(\Delta_j)$ can be calculated as

$$\zeta_z(\Delta_j) = \begin{cases} \zeta_z^+ = \vartheta_{sj}(\Delta_j/W_{sj}) / [1 - (\Delta_j/W_{sj})], & (\Delta_j \geq 0) \\ \zeta_z^- = \vartheta_{sj}(\Delta_j/W_{sj}) / [1 + (\Delta_j/W_{sj})], & (\Delta_j \leq 0) \end{cases} \quad (23)$$

Step 3: The following two compact sets are defined accordingly:

$$\mathcal{S}_{zj}^+ \stackrel{\text{def}}{=} \{(\zeta_j, \Delta_j) \in \mathbb{R}^2 \mid 0 < \zeta_j < \zeta_z^+, \Delta_j > 0\},$$

$$\mathcal{S}_{zj}^- \stackrel{\text{def}}{=} \{(\zeta_j, \Delta_j) \in \mathbb{R}^2 \mid \zeta_z^- < \zeta_j < 0, \Delta_j < 0\}.$$

Step 4: Substituting $E(\Delta_j, \zeta_j)\zeta_j$ around the domain $\mathcal{S}_{zj}^+ \cup \mathcal{S}_{zj}^-$, we can verify that, for $(\zeta_j, \Delta_j) \notin \mathcal{S}_{zj}^+ \cup \mathcal{S}_{zj}^-$, there is

$$E(\Delta_j, \zeta_j)\zeta_j < 0, \quad (24)$$

and for $(\zeta_j, \Delta_j) \in \mathcal{S}_{zj}^+ \cup \mathcal{S}_{zj}^-$, there is

$$E(\Delta_j, \zeta_j)\zeta_j > 0. \quad (25)$$

Using (21) and considering the extreme case when $K_j \rightarrow 0$, if $(\zeta_j, \Delta_j) \in \mathcal{S}_{zj}^+ \cup \mathcal{S}_{zj}^-$, \dot{V}_1 tends to be positive and ζ_j diverges from $\mathcal{S}_{zj}^+ \cup \mathcal{S}_{zj}^-$. By contrast, if $(\zeta_j, \Delta_j) \notin \mathcal{S}_{zj}^+ \cup \mathcal{S}_{zj}^-$, $\dot{V}_1 < 0$ and ζ_j converges back to $\mathcal{S}_{zj}^+ \cup \mathcal{S}_{zj}^-$. This variation proves that ζ_j is ultimately restricted within $\mathcal{S}_{zj}^+ \cup \mathcal{S}_{zj}^-$, which provides

$$|\zeta_j| \leq \vartheta_{sj}|\Delta_j/W_{sj}| / [1 + |\Delta_j/W_{sj}|]. \quad (26)$$

According to (23) and (26), if the candidates are chosen as $\vartheta_{sj} \ll 1$ and $W_{sj} \gg |\Delta_j|$, there exists $\zeta_z(\Delta_j)$ that tends to zero and satisfies the identity: $E(\Delta_j, \zeta_z(\Delta_j)) \equiv 0$. It illustrates that $F_{Aj}(\zeta_j)$ in (17) can effectively approximate the system nonlinearity $F_j(t)$ around the domain $\mathcal{S}_{zj}^+ \cup \mathcal{S}_{zj}^-$, while maintaining a small synthetic tracking error. \square

5. Adaptive Control Based on NINA

In this section, an adaptive control utilizing NINA is fulfilled, and the stability analysis is carried out.

5.1. Adaptive Law

Given that F_j and W_{sj} are optimal candidates for the approximation structure in (17), the integrated error $\iint E^2(\Delta_j, \zeta_j)d\Delta_j d\zeta_j$ is minimized. The estimation of $F_j(t)$ is defined as

$$\hat{F}_j(t) = \hat{F}_{Aj}(\zeta_j) = \hat{F}_{sj} + \hat{W}_{sj}\sigma(\zeta_j). \quad (27)$$

where \hat{F}_{sj} and \hat{W}_{sj} are the estimations of F_j and W_{sj} , respectively. Subtracting (27) from (16), the error between $F_j(t)$ and $\hat{F}_j(t)$ is represented as

$$\tilde{F}_j(t) = \tilde{F}_{sj} + \tilde{W}_{sj}\sigma(\xi_j) + E(\Delta_j, \xi_j), \quad (28)$$

with $\tilde{F}_{sj} = F_{sj} - \hat{F}_{sj}$ and $\tilde{W}_{sj} = W_{sj} - \hat{W}_{sj}$. The adaptive law of \hat{F}_{sj} and \hat{W}_{sj} is given by the following squared-error correction procedures:

$$\dot{\hat{W}}_{sj} = -A_j\tilde{\xi}_j^2\hat{W}_{sj} + B_j\sigma(\xi_j)\xi_j \quad (29)$$

$$\dot{\hat{F}}_{sj} = -A_j\tilde{\xi}_j^2\hat{F}_{sj} + B_j\xi_j \quad (30)$$

where $A_j, B_j > 0$ are the adaptive gains. The term $A_j\tilde{\xi}_j^2$ plays a role in preventing the divergences of \hat{W}_{sj} and \hat{F}_{sj} .

Using (29) and (30), the transient performance of \tilde{F}_{sj} and \tilde{W}_{sj} is analyzed next. Applying $\dot{\tilde{W}}_{sj} = -\dot{\hat{W}}_{sj}$ and $\dot{\tilde{F}}_{sj} = -\dot{\hat{F}}_{sj}$, (29) and (30) can then be represented as

$$\dot{\tilde{W}}_{sj} = -A_j\tilde{\xi}_j^2\tilde{W}_{sj} + \rho(\xi_j), \quad (31)$$

$$\dot{\tilde{F}}_{sj} = -A_j\tilde{\xi}_j^2\tilde{F}_{sj} + \varrho(\xi_j), \quad (32)$$

where

$$\rho = (A_j\xi_j W_{sj} - B_j\sigma(\xi_j))\xi_j, \varrho = (A_j\xi_j F_{sj} - B_j)\xi_j.$$

The solutions of (31) and (32) are represented as

$$\tilde{W}_{sj}(t) = \phi(t, t_1)\tilde{W}_{sj}(t_1) + \int_{t_1}^t \phi(t, \tau)\rho(\tau)d\tau, \quad (33)$$

$$\tilde{F}_{sj}(t) = \phi(t, t_1)\tilde{F}_{sj}(t_1) + \int_{t_1}^t \phi(t, \tau)\varrho(\tau)d\tau, \quad (34)$$

where

$$\phi(t, t_1) = \exp\left(-A_j \int_{t_1}^t \tilde{\xi}_j^2(\tau)d\tau\right). \quad (35)$$

Supposing that the persistent excitation condition holds for ξ_j , $\phi(t, t_1)$ asymptotically converges to zero with the increase in t , proving that (31) and (32) are bounded-input-bounded-output stable. The expressions of ρ and ϱ show that ξ_j is a unique source that changes \tilde{W}_{sj} and \tilde{F}_{sj} in the steady state. Therefore, \tilde{W}_{sj} and \tilde{F}_{sj} can be restricted within a small area along with the convergence of ξ_j . We can also conclude from (35) that \tilde{W}_{sj} and \tilde{F}_{sj} obtain fast convergence as long as A_j is set to make the steady-state time of $\phi(t, t_1)$ much smaller than μT_c .

5.2. Adaptive Controller and Stability Analysis

Combining the control structure in (12), and approximating the system nonlinearity using (27), (29), and (30), the NINA-based adaptive control law is presented as

$$\begin{cases} \tau_j = K_j\xi_j + \hat{F}_{sj} + \hat{W}_{sj}\sigma(\xi_j) \\ \dot{\hat{W}}_{sj} = -A_j\tilde{\xi}_j^2\hat{W}_{sj} + B_j\sigma(\xi_j)\xi_j \\ \dot{\hat{F}}_{sj} = -A_j\tilde{\xi}_j^2\hat{F}_{sj} + B_j\xi_j \end{cases} \quad (36)$$

Theorem 2. Consider the nonlinear system represented by (3) and use the control law in (36). If control gain K_j is selected in accordance with the following inequality

$$K_j > \frac{1}{4} \left[A_j \left(W_{sj}^2 + F_{sj}^2 \right) / B_j \right], \tag{37}$$

the synthetic tracking $\tilde{\xi}_j$ is uniformly and ultimately bounded by

$$|\tilde{\xi}_j|^2 \leq W_{sj} \vartheta_{sj} / G_j$$

with

$$G_j = K_j - \frac{1}{4} \left[A_j \left(W_{sj}^2 + F_{sj}^2 \right) / B_j \right]$$

Moreover, the synthetic tracking error $\tilde{\xi}_j$ can be restricted to a small area around zero as $0 < (\vartheta_{sj}, A_j) \ll 1$ and $(K_j, B_j) \gg 1$.

Proof. A Lyapunov function candidate is selected as

$$V_2 = V_1 + \frac{1}{2B_j} \sum_j \left(\tilde{W}_{sj}^2 + \tilde{F}_{sj}^2 \right), \tag{38}$$

Using (13) and differentiating (38) with respect to time, we have

$$\dot{V}_2 = \sum_j \left[\tilde{\xi}_j \tilde{F}_j(t) + \left(\tilde{W}_{sj} \dot{\tilde{W}}_{sj} + \tilde{F}_{sj} \dot{\tilde{F}}_{sj} \right) / B_j - K_j \tilde{\xi}_j^2 \right], \tag{39}$$

Applying $\dot{\tilde{W}}_{sj} = -\dot{W}_{sj}$ and $\dot{\tilde{F}}_{sj} = -\dot{F}_{sj}$ with (29) and (30), \dot{V}_2 becomes

$$\dot{V}_2 = \sum_j \left[A_j \tilde{\xi}_j^2 \left(\tilde{W}_{sj} \hat{W}_{sj} + \tilde{F}_{sj} \hat{F}_{sj} \right) / B_j + E_j(\Delta_j, \tilde{\xi}_j) \tilde{\xi}_j - K_j \tilde{\xi}_j^2 \right]. \tag{40}$$

where $\tilde{W}_{sj} \hat{W}_{sj}$ and $\tilde{F}_{sj} \hat{F}_{sj}$ are bounded by

$$\tilde{W}_{sj} \hat{W}_{sj} \equiv \tilde{W}_{sj} \left(W_{sj} - \tilde{W}_{sj} \right) \leq W_{sj}^2 / 4, \tag{41}$$

$$\tilde{F}_{sj} \hat{F}_{sj} \equiv \tilde{F}_{sj} \left(F_{sj} - \tilde{F}_{sj} \right) \leq F_{sj}^2 / 4. \tag{42}$$

Substituting (41) and (42) into (40), we can obtain the following inequality:

$$\dot{V}_2 \leq -\sum_j G_j \tilde{\xi}_j^2 + \sum_j E(\Delta_j, \tilde{\xi}_j) \tilde{\xi}_j, \tag{43}$$

where $G_j = K_j - \frac{1}{4} \left[A_j \left(W_{sj}^2 + F_{sj}^2 \right) / B_j \right]$.

According to the conclusion in (22) that $E(\Delta_j, \tilde{\xi}_j) \tilde{\xi}_j$ is an open-downward convex function with respect to $\tilde{\xi}_j$, $E(\Delta_j, \tilde{\xi}_j) \tilde{\xi}_j$ will reach its maximum value as

$$\frac{\partial E(\Delta_j, \tilde{\xi}_j) \tilde{\xi}_j}{\partial \tilde{\xi}_j} = 0. \tag{44}$$

Substituting the solution of (44), the maximum value of $E(\Delta_j, \xi_j) \xi_j$ can be calculated as

$$E(\Delta_j, \xi_j) \xi_j \leq W_{sj} \sigma^2(\xi_j) \vartheta_{sj} = W_{sj} \vartheta_{sj} \xi_j^2 / (\vartheta_{sj} + |\xi_j|)^2. \quad (45)$$

Applying (45), (43) becomes

$$\dot{V}_2 \leq -\sum_j G_j \xi_j^2 + \sum_j \left[W_{sj} \vartheta_{sj} / (\vartheta_{sj} + |\xi_j|) \right]^2 \xi_j^2. \quad (46)$$

If $|\xi_j|^2 > \frac{W_{sj} \vartheta_{sj}}{G_j}$, we have $\dot{V}_2 < 0$. Hence, the synthetic tracking error ξ_j is uniformly and ultimately bounded by

$$|\xi_j|^2 \leq W_{sj} \vartheta_{sj} / G_j. \quad (47)$$

The synthetic tracking error ξ_j will be restricted into a small area around zero as $0 < (\vartheta_{sj}, A_j) \ll 1$ and $(K_j, B_j) \gg 1$. This completes the proof. \square

6. Numerical Simulation

In this section, the proposed method is verified by the trajectory tracking control of a two-link flexible-joint manipulator. The simulations of the manipulator under step change, different link lengths, and joint stiffness are performed to evaluate the robustness of the proposed method. The simulations are conducted utilizing the fourth-order Runge–Kutta method.

The finite-time sliding mode control (FT-SMC) in [46] and the RBFN-based control in [51] are also simulated for comparison. These two controllers are selected as representatives of sliding mode control and RBFN-based control methods. They exhibit relatively simple yet representative architectures and are also model-free methods, which makes them suitable as benchmarks for comparison.

6.1. Simulation Setup

The configuration of the manipulator is depicted in Figure 3, and its parameters are listed in Table 1. Referring to [52], the system dynamics can be modeled as

$$\begin{bmatrix} m_{11}(\alpha_1, \alpha_2) & m_{12}(\alpha_1, \alpha_2) \\ m_{21}(\alpha_1, \alpha_2) & m_{22}(\alpha_1, \alpha_2) \end{bmatrix} \begin{bmatrix} \ddot{\alpha}_1 \\ \ddot{\alpha}_2 \end{bmatrix} + \begin{bmatrix} h_1 \\ h_2 \end{bmatrix} + \begin{bmatrix} G_1 \\ G_2 \end{bmatrix} = \begin{bmatrix} u_1 \\ u_2 \end{bmatrix} \quad (48)$$

$$\begin{bmatrix} J_1(\beta_1) & 0 \\ 0 & J_2(\beta_2) \end{bmatrix} \begin{bmatrix} \ddot{\beta}_1 \\ \ddot{\beta}_2 \end{bmatrix} + \begin{bmatrix} f_{d1} \\ f_{d2} \end{bmatrix} - \begin{bmatrix} u_1 \\ u_2 \end{bmatrix} = \begin{bmatrix} \tau_3 \\ \tau_4 \end{bmatrix} \quad (49)$$

with

$$\begin{cases} u_1 = k_{s1}(\alpha_1 - \beta_1) + k_{d1}(\dot{\alpha}_1 - \dot{\beta}_1) \\ u_2 = k_{s2}(\alpha_2 - \beta_2) + k_{d2}(\dot{\alpha}_2 - \dot{\beta}_2) \end{cases} \quad (50)$$

where $\alpha = (\alpha_1, \alpha_2)^T$ and $\beta = (\beta_1, \beta_2)^T$ are the position vectors of the load and motor sides, respectively; $m_{11}, m_{12}, m_{21}, m_{22}$ are the elements of the load side inertial matrix, J_1 and J_2 are the elements of the motor side inertial matrix; h_1 and h_2 consist of Coriolis and centrifugal terms; G_1 and G_2 contain gravitational terms; u_1 and u_2 are the elastic torque terms; f_{d1} and f_{d2} are the damping terms of the motor side; and τ_3 and τ_4 are the motor torques.

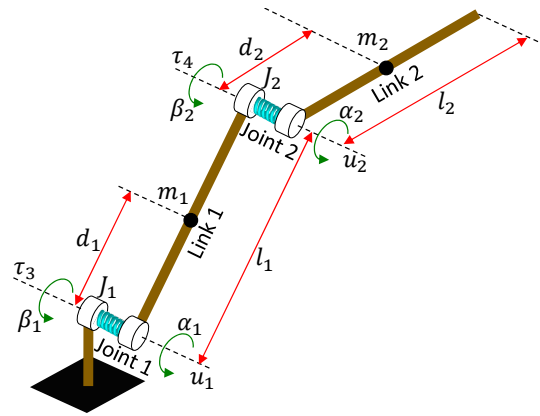


Figure 3. Architecture of the two-link robot manipulator with joint flexibility.

Table 1. Parameters of the two-link robot manipulator system.

Parameters	Value	Parameters	Value	Unit	Means
m_1	6.0	m_2	4.0	kg	mass of the link
l_1	0.6	l_2	0.4	m	length of the link
d_1	0.3	d_2	0.2	m	length of the mass center
J_1	2.2×10^{-3}	J_2	6.4×10^{-4}	kg.m ²	motor inertia
f_{d1}	0.088	f_{d2}	0.057	N.m/rad/s	motor damping
k_{s1}	120.0	k_{s2}	100.0	N.m/rad	joint stiffness
k_{d1}	6.79×10^{-2}	k_{d2}	3.69×10^{-2}	N.m/rad/s	elasticity damping

The control law presented in Theorem 2 is applied. The reference trajectory of the load-side is given by the user command. The reference trajectory of the motor side is generated by solving the following differential equation:

$$\begin{cases} \dot{\beta}_{r1} = -k_{s1}\beta_{r1}/k_{d1} + [(\tau_{\alpha1} + k_{s1}\alpha_1)/k_{d1} + \dot{\alpha}_1] \\ \dot{\beta}_{r2} = -k_{s2}\beta_{r2}/k_{d2} + [(\tau_{\alpha2} + k_{s2}\alpha_2)/k_{d2} + \dot{\alpha}_2] \end{cases} \quad (51)$$

where $(\beta_{r1}, \beta_{r2}, \dot{\beta}_{r1}, \dot{\beta}_{r2})$ represent the command trajectory of the motor side, and $\tau_{\alpha1}$ and $\tau_{\alpha2}$ are the desired values of u_1 and u_2 , respectively. This formula is an inverse mapping of $u_1(\alpha_1, \dot{\alpha}_1, \beta_{1r}, \dot{\beta}_{1r})$ and $u_2(\alpha_2, \dot{\alpha}_2, \beta_{2r}, \dot{\beta}_{2r})$ in (50). The parameters of the proposed adaptive controller used in the simulation are listed in Table 2.

Table 2. Parameters of the proposed NINA-based adaptive control.

Parameters	Value	Parameters	Value
$\vartheta_{s1}, \vartheta_{s2}$	0.3	$\vartheta_{s3}, \vartheta_{s4}$	6
$K_1 \sim K_2$	10	$K_3 \sim K_4$	5
$A_1 \sim A_2$	0.3	$A_3 \sim A_4$	1
$B_1 \sim B_2$	1000	$B_3 \sim B_4$	1000
$\Lambda_1 \sim \Lambda_2$	5	$\Lambda_3 \sim \Lambda_4$	5

Note that subscripts 1 and 2 represent the motor-side control parameters of joints 1 and 2, respectively. Subscripts 3 and 4 represent the load-side control parameters of joints 1 and 2, respectively.

Remark 4. For the flexible joint system mentioned above, the motor side is the actuated subsystem, and the link side is the unactuated subsystem. The elastic torque (u_1, u_2) helps coordinate the behavior of the motor and load sides. It can be verified that Assumptions 1 and 2 hold for (u_1, u_2) by examining the expression in (50).

6.2. Trajectory Tracking Performance Validation

We compared the trajectory tracking performance of the three control methods: the proposed method, the RBFN-based method, and FT-SMC. The robot arm starts from the horizontal position and tracks sinusoidal trajectories as shown below:

$$\begin{cases} \alpha_r = \frac{\pi}{6}(1 + \sin(2t)), \text{ load side} \\ \beta_r = \frac{\pi}{6}(1 + \cos(2t)), \text{ motor side} \end{cases}$$

To evaluate the tracking performance of the controllers, we introduce the following evaluation index, and the results are listed in Tables 3 and 4:

Table 3. Tracking performance of the three methods.

		SSP		CTP		
		Joint 1	Joint 2	Joint 1	Joint 2	Average
Link Side	NINA	−0.07°~−0.08°	−0.03°~−0.03°	1.75 s	1.78 s	1.77 s
	FT-SMC	−0.05°~−0.09°	−0.07°~−0.10°	1.88 s	1.24 s	1.56 s
	RBFN	−0.17°~−0.16°	0.20°~−0.20°	2.73 s	1.74 s	2.24 s
Motor Side	NINA	−0.11°~−0.12°	−0.13°~−0.13°	0.50 s	0.20 s	0.35 s
	FT-SMC	−0.21°~−0.09°	−0.07°~−0.10°	0.82 s	0.90 s	0.86 s
	RBFN	−0.29°~−0.17°	−0.18°~−0.19°	1.24 s	1.09 s	1.17 s

Table 4. Nonlinearity estimation performance of the three methods.

		SSE		CTE		
		Joint 1	Joint 2	Joint 1	Joint 2	Average
Link Side	NINA	−0.078~−0.16 Nm	−0.12~−0.11 Nm	0.7 s	0.4 s	0.55 s
	FT-SMC	−0.28~−0.50 Nm	−0.19~−0.19 Nm	1.9 s	1.7 s	1.8 s
	RBFN	−1.60~−1.60 Nm	−0.8~−0.8 Nm	2.76 s	1.9 s	2.33 s
Motor Side	NINA	−0.27~−0.52 Nm	−0.064~−0.006 Nm	0.24 s	0.19 s	0.22 s
	FT-SMC	−1.05~−0.75 Nm	−0.14~−0.14 Nm	0.9 s	1.3 s	1.10 s
	RBFN	−2.14~−0.55 Nm	−0.66~−0.64 Nm	1.2 s	1.4 s	1.30 s

(a) SSP (steady-state tracking error in position):

$$SSP = [\min e_j(t) \max e_j(t)], \text{ for } t > t_{M1}, j = \alpha \text{ or } \beta$$

where $\min e_j(t)$ and $\max e_j(t)$ represent the lower and upper bounds of the position tracking error, respectively. t_{M1} represents the time since the tracking error varied periodically and steadily. In this simulation, it is set $t_{M1} = 4$ s.

(b) CTP (convergence time of trajectory tracking): It is defined as the time when the tracking error is free from initial oscillation, shown in Figure 4c, and first comes into the range of steady-state, i.e., SSP.

(c) SSE (steady-state estimation error in system nonlinearity):

$$SSE = [\min \tilde{F}_j(t) \max \tilde{F}_j(t)], \text{ for } t > t_{M2}, j = \alpha \text{ or } \beta$$

where $\min \tilde{F}_j(t)$ and $\max \tilde{F}_j(t)$ represent the low and up bounds of the nonlinearity estimation error, respectively. t_{M2} is defined similarly to t_{M1} and is set as $t_{M2} = 4$ s.

(d) CTE (convergence time of nonlinearity estimation): It is similar to the definition of CTP.

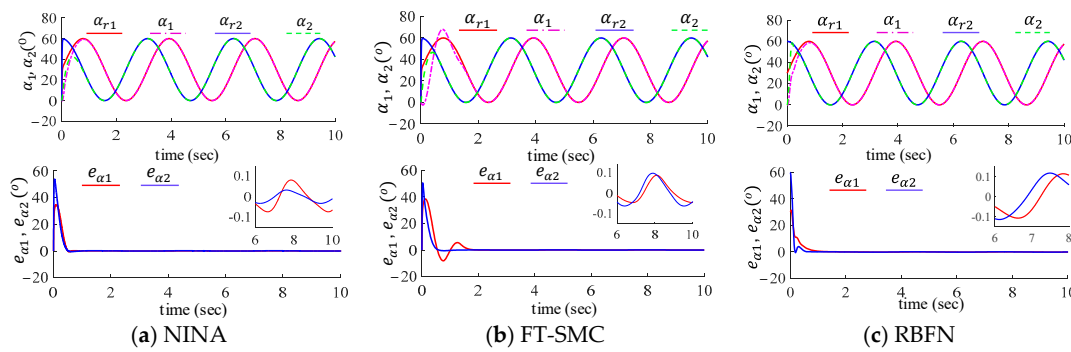


Figure 4. Link-side tracking performance of (a) the proposed method, (b) FT-SMC, and (c) RBFN.

The tracking performance of the three controllers is illustrated in Figures 4 and 5. The steady-state tracking accuracy and convergence time are listed in Table 3. All three controllers can effectively track sinusoidal trajectories. Among them, the proposed algorithm exhibits smooth and fast convergence during the transient phase, while the other two methods show more pronounced oscillations. This is due to excessive control gain. As shown in Table 3, the tracking errors of the proposed control algorithm on the load side for joints 1 and 2 are, respectively $-0.07^{\circ} \sim 0.08^{\circ}$ and $-0.03^{\circ} \sim 0.03^{\circ}$; on the motor side, the tracking errors are $-0.11^{\circ} \sim 0.12^{\circ}$ and $-0.13^{\circ} \sim 0.13^{\circ}$, respectively. The overall steady-state tracking accuracy of the proposed algorithm is superior to the other two control algorithms.

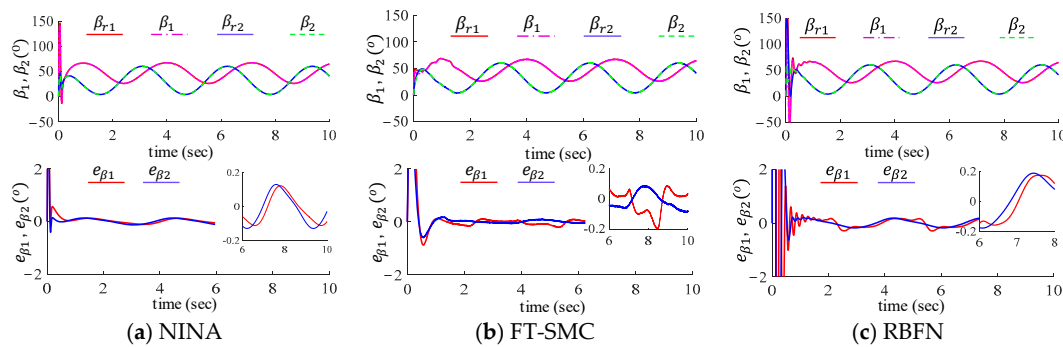


Figure 5. Motor-side tracking performance of (a) the proposed method, (b) FT-SMC, and (c) RBFN.

It can be seen from Figure 6 and Table 4 that the proposed algorithm achieves faster convergence of the nonlinear approximation error than the other two methods. This verifies its ability to track unknown disturbances with high dynamics. In addition, the proposed method also illustrates the high estimation accuracy of system nonlinearity.

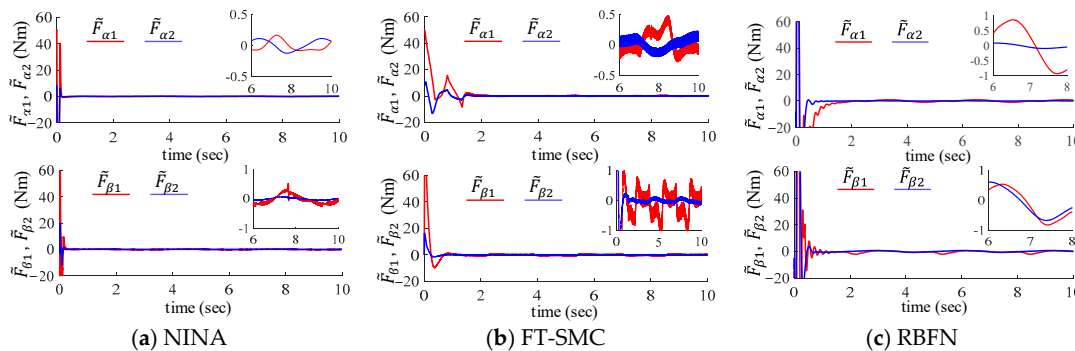


Figure 6. Approximation errors of the unknown system nonlinearity using (a) the proposed method, (b) the FT-SMC, and (c) the RBFN method.

Finally, the control signals of the three controllers are depicted in Figure 7. The control inputs of the proposed method and the RBFN-based method are milder, while the one of the FT-SMC shows significant chattering, especially on the motor side. It is a typical problem for sliding mode control. Compared with the traditional SMC method, the FT-SMC presented in [46] solved the peak phenomenon and suppressed the control chattering by asymptotical convergence, which is a considerable contribution. However, for nonlinear cascaded systems such as the flexible-joint manipulator, the control input of the outer loop (the load side) is usually mapped as the command of the inner loop (the motor side). This mapping process transmits the small chattering on the load side into the command layer of the motor side. The suppressed chattering is then amplified again by the motor-side control loop. As verified in Figure 7, the control input of the motor side contains obvious chattering, while the control input of the load side is milder.

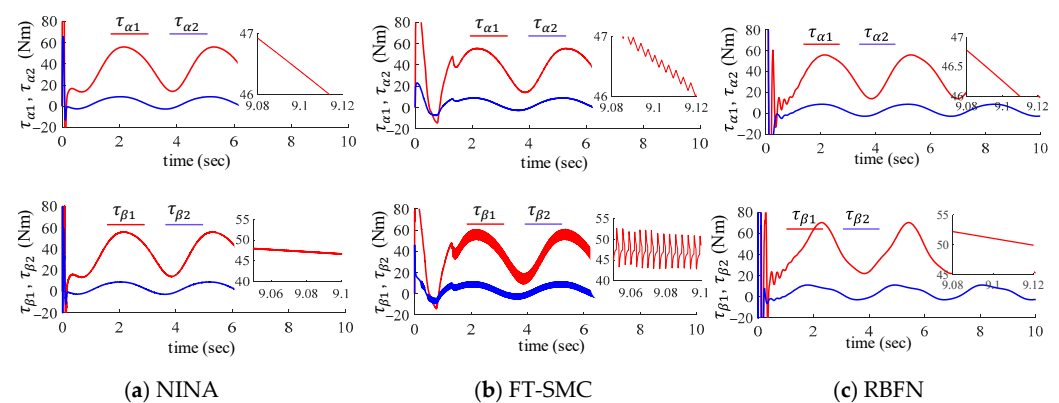


Figure 7. Control efforts of the proposed method (**top row**), the FT-SMC (**middle column**), and the RBFN method (**bottom row**).

In summary, the FT-SMC control shows good trajectory tracking accuracy and nonlinear estimation accuracy, but significant chattering occurs, which can lead to the failure of precision sensors and actuators in practical applications. Neural network-based control such as the RBFN-based method shows relatively lower convergence speed for nonlinearity approximation due to its comparably complex topology. In contrast, the proposed algorithm adopts a simple and effective estimation structure, which not only shows the ability for fast and accurate nonlinearity approximation but also maintains mild control input. This is also the major motivation for our research on this algorithm.

6.3. Robustness Validation

As shown in Figure 8, to further verify the stability and robustness of the proposed control, we examined the step response of the proposed method and its ability to recover from sudden disturbances. It can be observed that when encountering step changes, each joint can quickly track the new reference signal. The settling times for joints 1 and 2 are 0.618 s and 0.60 s, respectively. A 10 Nm impulse disturbance is introduced at 4 s and revoked at 6 s. It can be seen that the system can recover tracking of the original position within 2 s and has the ability to maintain a fixed point position with high precision (position tracking error $< 1 \times 10^{-5}$ degree).

Figure 9 compares the tracking performance of the proposed control method under different link lengths. Although the load environment has changed, the proposed adaptive control maintains high tracking performance. Figure 10 illustrates the dynamic behavior of the whole system under different joint stiffnesses. It is illustrated that all the synthetic tracking errors and nonlinearity estimation errors uniformly and asymptotically converge toward zero, regardless of the variation of the joint stiffness. These results verify the effectiveness and robustness of the proposed method.

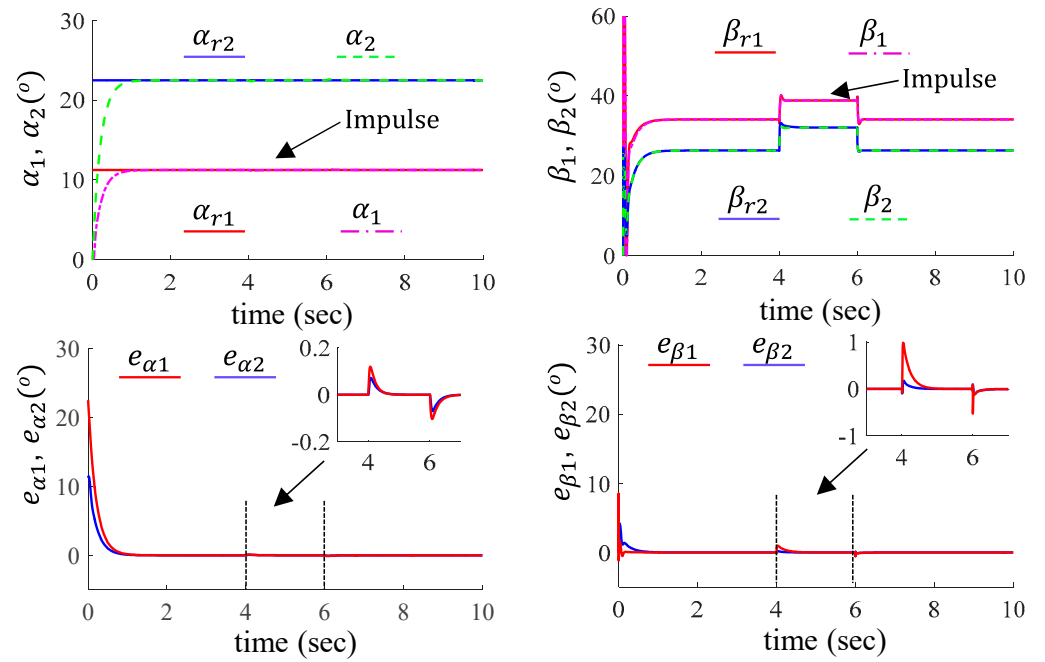


Figure 8. Tracking performance of the proposed method under step change and impulse disturbance. The first row shows the position of the load and motor sides, and the second row shows their tracking errors.

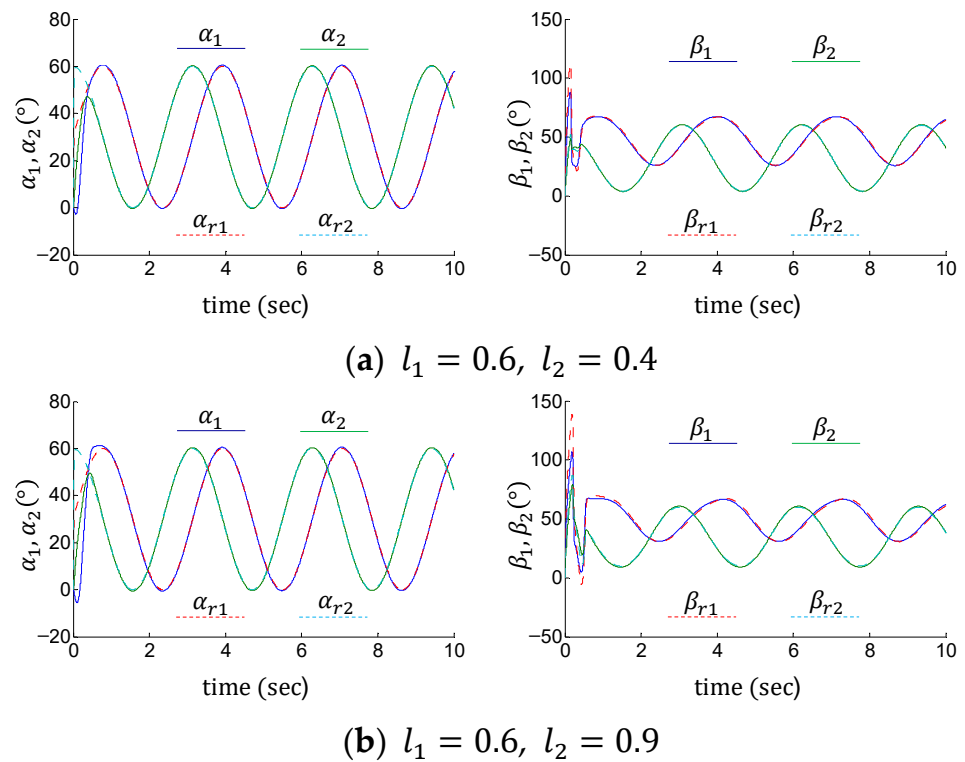


Figure 9. Results of tracking control under different link lengths using the proposed control method.

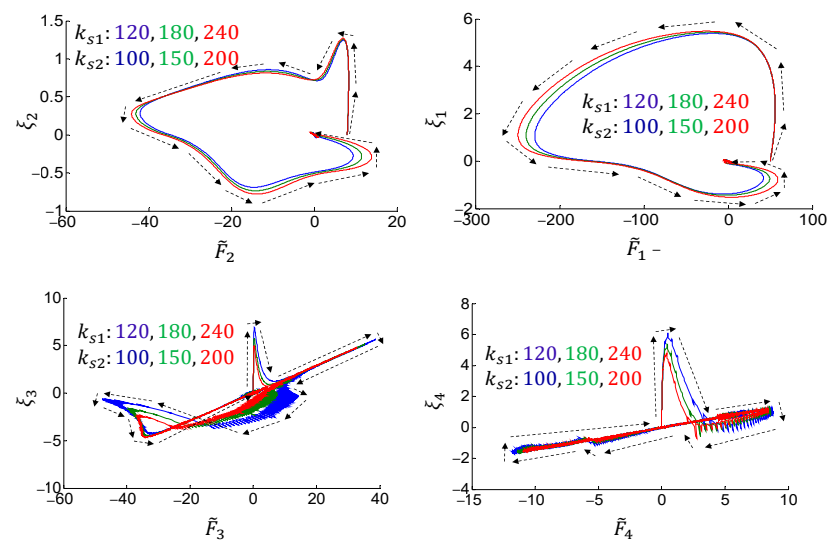


Figure 10. Dynamic behavior of the manipulator under different joint stiffness using the proposed control method.

7. Experiments

In this section, the proposed control method is further validated on a flexible-joint platform. The RBFN-based adaptive control method in [51] is introduced for comparison. Trajectory tracking experiments under different end loads are conducted.

7.1. Experiment Setup

Figure 11 shows a typical flexible-joint platform. From the left to right sides, there are a servo motor, a harmonic drive (with a 50:1 gear ratio), a flexible body, a torque sensor, and an output link with an end load. The flexible body here is a series of elastic actuators. The angular positions of load side α and motor side β are measured by optical encoders. The generated torque command τ_β is implemented through a servo driver. The torque sensor and signal detection-conversion card are employed to measure the output torque of load side τ_l and motor side τ_m , respectively. The nominal parameters of the platform are obtained via parameter identification and measurement, which are listed in Table 5.

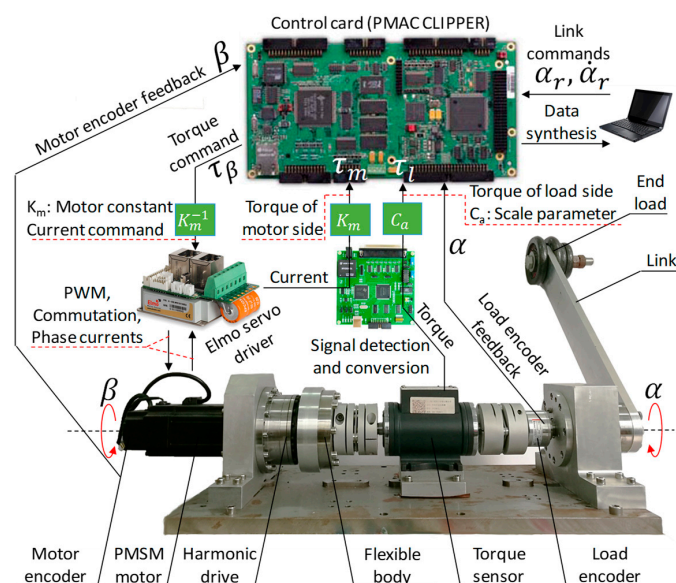


Figure 11. Architecture of the experimental system.

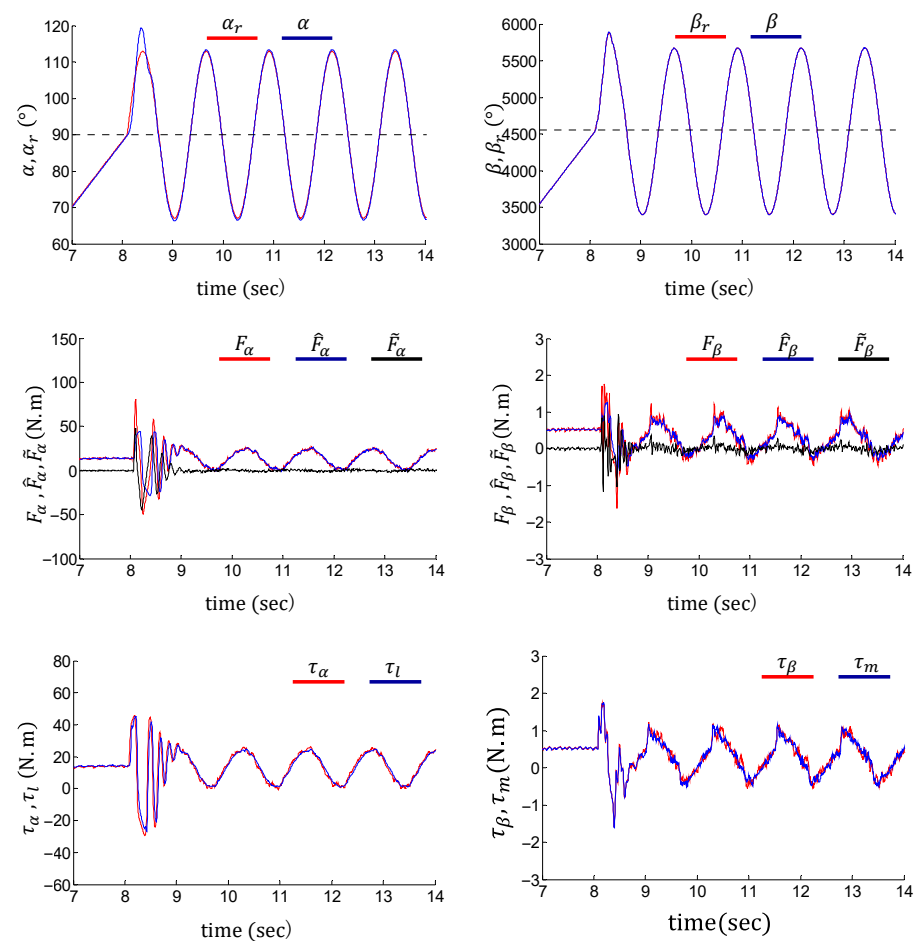
Table 5. Parameters of the flexible joint system.

Measured Values of Mechanical Parameters			Control Parameters			
J_α	1.090, under 2 kg end load	kg.m ²	ϑ_{s1}	1.125000	ϑ_{s2}	0.030000
	1.840, under 4 kg end load	kg.m ²	K_1	0.135000	K_2	0.010000
g_α	15.12, under 2 kg end load	N.m	Λ_1	26.50000	Λ_2	200.0000
	24.08, under 4 kg end load	N.m	A_1	0.000180	A_2	0.000001
J_β	4.65×10^{-4}	kg.m ²	λ_1	125000.0	λ_2	100000.0
k_s	927.0	N.m/rad				
k_d	1.54	N.m/rad/sec				
η	50.0	—				

Note that subscripts α and β represent the load and motor sides of the flexible-joint platform, respectively.

7.2. Experimental Results

Figures 12 and 13 show the tracking performance, nonlinearity approximations, and control inputs of the flexible joint using the proposed control method under 2 kg and 4 kg load conditions, respectively. The link action is set as follows: The initial posture of the link is vertically downward. It first rotates at a constant speed of $18^\circ/\text{s}$ toward the horizontal level, then swings around the horizontal position. The swing amplitude and frequency are 21.6° and 0.8 Hz, respectively. The black dotted lines in the left column of Figure 12 indicate the horizontal position. The experimental results verify the tracking performance of the control system under both ramp and harmonic trajectories. The entire process is divided into three phases, i.e., the ramping phase, the switching phase, and the waving phase. The system exhibits transient responses in the switching phase (8 s to 10 s), due to the discontinuity of the velocity command $\dot{\alpha}_r$.

**Figure 12.** Performance of NINA-based adaptive control under a 2 kg end load.

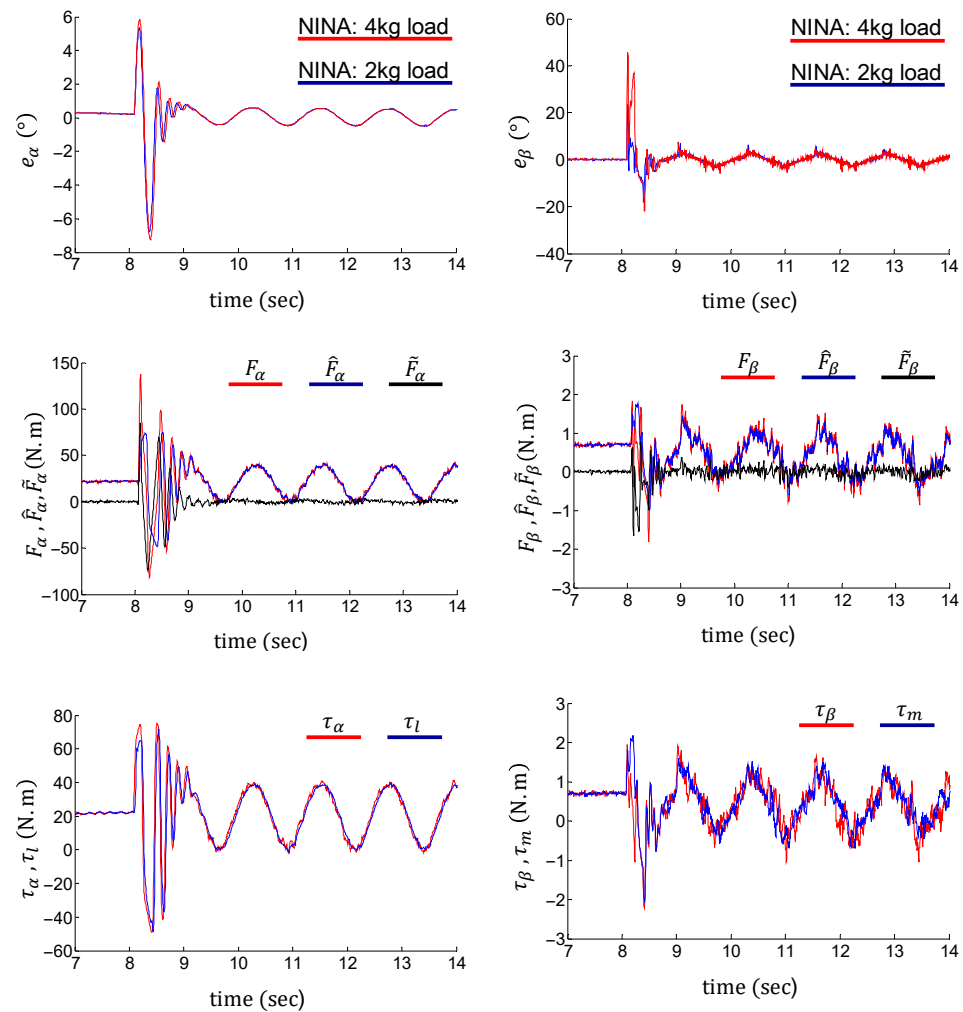


Figure 13. Performance of NINA-based adaptive control under a 4 kg end load.

As shown in the first rows of Figures 12 and 13, the control system stabilizes within 1 s during the switching phase. Tracking errors are limited within 0.5° and 10° on the load and motor sides (with a 50:1 gear ratio) during the ramping and waving phases, respectively. Although the flexible joint waves vertically under an end load, the tracking errors do not contain obvious biases.

The second rows of Figures 12 and 13 show accurate nonlinearity approximations, which validate the effectiveness of the NINA technique. The third rows of Figures 12 and 13 indicate that the above control performances are achieved under relatively clean control inputs. It is noteworthy that the tracking errors under different end loads are nearly identical. This verifies the robustness of the proposed control method.

A classical RBFN-based adaptive control presented in [51] is compared with the proposed control method. On the load side, $\Lambda_1 e_\alpha + \dot{\alpha}_r$, $\Lambda_1 \dot{e}_\alpha + \ddot{\alpha}_r$, α , and $\dot{\alpha}$ are supplied to the input layer of RBFN. On the motor side, $\Lambda_2 e_\beta + \dot{\beta}_r$, $\Lambda_2 \dot{e}_\beta + \ddot{\beta}_r$, β , and $\dot{\beta}$ are supplied to the input layer of RBFN. Five neurons are set in hidden layers on the load side and the motor side. The control torques are obtained from the output layer of the RBFN. For more details, please refer to [51].

The performance of RBFN control is shown in Figure 14. In the switching phase, the tracking error of the proposed method converges faster than the RBFN-based method. In the swing phase, the load- and motor-side tracking errors of the RBFN control are bounded by $|e_\alpha| < 1.75^\circ$ and $|e_\beta| < 3^\circ$, respectively. The tracking errors of the proposed NINA-based control method are bounded by $|e_\alpha| < 0.25^\circ$ and $|e_\beta| < 3^\circ$. In addition, the nonlinearity approximation of the RBFN control (\hat{F}_α , \hat{F}_β) shows obvious lags behind their nominal

values (F_α, F_β) , thereby resulting in relatively large estimation errors $(\tilde{F}_\alpha, \tilde{F}_\beta)$. The above comparison indicates that the proposed NINA-based adaptive control can realize better control performance than the RBFN-based adaptive control on the flexible joint system.

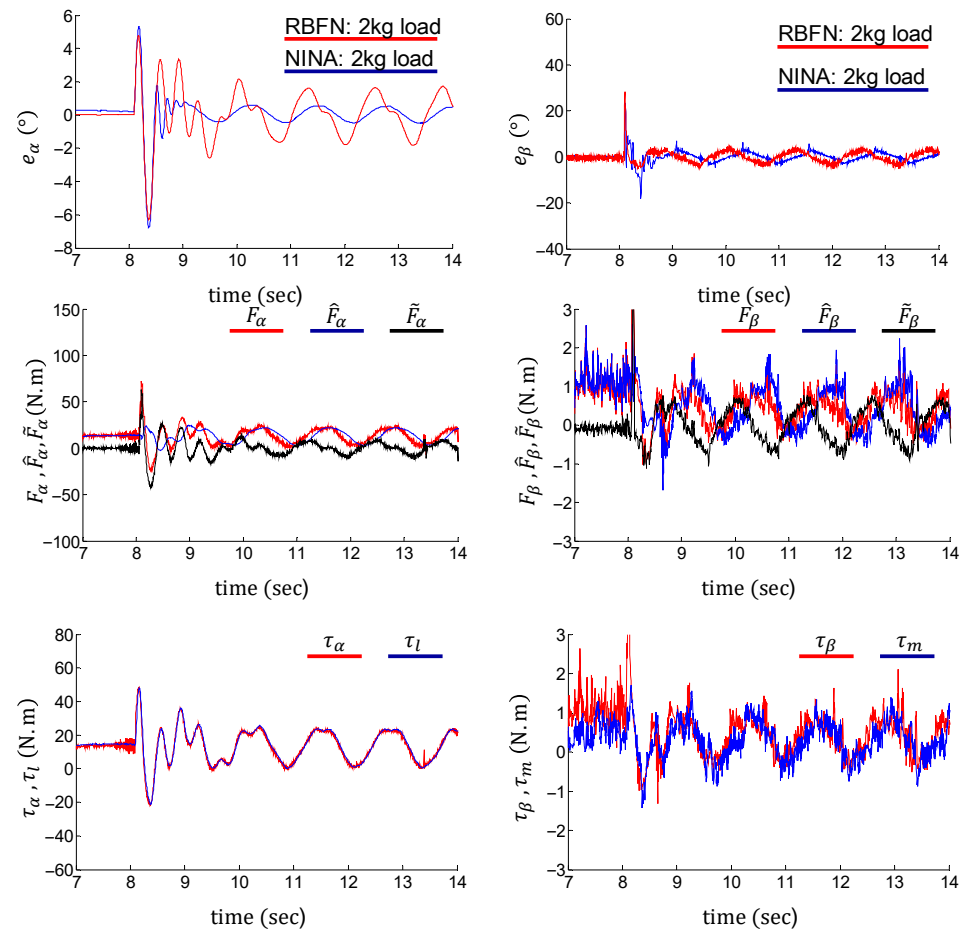


Figure 14. Performance of the RBFN adaptive controller under a 2 kg end load.

8. Conclusions

This study proposed a simplified adaptive control based on NINA for a class of nonlinear cascaded systems. The uniformity and ultimate stability of the proposed control were proven. The nonlinearities of each subsystem were approximated using the synthetic form of a steady component and an alternating component based only on local tracking errors. The proposed control method was validated through applications on the flexible joint system involving numerical simulations and experiments. The simulation results illustrated that the proposed method can achieve similar control accuracy as FT-SMC but uses milder control inputs. It was also indicated that the proposed method is insensitive to external loads and parametric perturbations. The proposed method was compared with an RBFN-based method. The experimental results demonstrated that the proposed method could achieve better control performance than an RBFN-based method.

Future work could be extended to flexible manipulators with variable stiffness. Future interests lie in two main areas: The first is optimizing the mapping process from the control input of the unactuated subsystem to the command layer of the actuated subsystem, which could improve the stability and noise level of the control system. The second is augmenting the adaptive law with a priori information on the system, to accelerate the convergence of the nonlinearity approximation.

Author Contributions: Conceptualization, Z.L.; formal analysis, Z.L.; methodology, Z.L. and H.J.; project administration, J.Z.; supervision, J.Z.; validation, Z.L.; writing—original draft, Z.L.; writing—review and editing, Z.L. and H.J. All authors have read and agreed to the published version of the manuscript.

Funding: The authors gratefully acknowledge the financial support of the National Natural Science Foundation of China under Grants 62373121, STI 2030-Major Projects 2021ZD0201400, and the National Natural Science Foundation of China under Grants 92048301.

Institutional Review Board Statement: Not applicable.

Informed Consent Statement: Not applicable.

Data Availability Statement: Data are contained within the article.

Conflicts of Interest: The authors declare no conflict of interest.

References

- Han, S.I.; Lee, J.M. Fuzzy Echo State Neural Networks and Funnel Dynamic Surface Control for Prescribed Performance of a Nonlinear Dynamic System. *IEEE Trans. Ind. Electron.* **2014**, *61*, 1099–1112. [[CrossRef](#)]
- Jin, H.; Lee, J. An RMRAC Current Regulator for Permanent-Magnet Synchronous Motor Based on Statistical Model Interpretation. *IEEE Trans. Ind. Electron.* **2009**, *56*, 169–177. [[CrossRef](#)]
- Le-Tien, L.; Albu-Schäffer, A. Robust Adaptive Tracking Control Based on State Feedback Controller with Integrator Terms for Elastic Joint Robots with Uncertain Parameters. *IEEE Trans. Control Syst. Technol.* **2018**, *26*, 2259–2267. [[CrossRef](#)]
- Xu, J.X.; Guo, Z.Q.; Lee, T.H. Design and Implementation of Integral Sliding-Mode Control on an Underactuated Two-Wheeled Mobile Robot. *IEEE Trans. Ind. Electron.* **2014**, *61*, 3671–3681. [[CrossRef](#)]
- Han, S.I.; Lee, J.M. Balancing and Velocity Control of a Unicycle Robot Based on the Dynamic Model. *IEEE Trans. Ind. Electron.* **2015**, *62*, 405–413. [[CrossRef](#)]
- Jin, H.; Hwang, J.; Lee, J. A Balancing Control Strategy for a One-Wheel Pendulum Robot Based on Dynamic Model Decomposition: Simulations and Experiments. *IEEE-ASME Trans. Mechatron.* **2011**, *16*, 763–768. [[CrossRef](#)]
- Cho, S.K.; Jin, H.Z.; Lee, J.M.; Yao, B. Teleoperation of a Mobile Robot Using a Force-Reflection Joystick with Sensing Mechanism of Rotating Magnetic Field. *IEEE-ASME Trans. Mechatron.* **2010**, *15*, 17–26. [[CrossRef](#)]
- Zhu, Y.H.; Gao, Y.S.; Xu, C.H.; Zhao, J.; Jin, H.Z.; Lee, J. Adaptive Control of a Gyroscopically Stabilized Pendulum and Its Application to a Single-Wheel Pendulum Robot. *IEEE-ASME Trans. Mechatron.* **2015**, *20*, 2095–2106. [[CrossRef](#)]
- Zhu, Y.H.; Li, G.; Zhao, J.; Jin, H.Z. Attitude-Guided Robust Adaptive Path Following Control for Ducted Fan UAV. In Proceedings of the 2014 IEEE International Conference on Robotics and Automation (ICRA), Hong Kong, China, 31 May–7 June 2014; pp. 31–36.
- Miranda-Colorado, R.; Aguilar, L.T. Robust PID control of quadrotors with power reduction analysis. *ISA Trans.* **2020**, *98*, 47–62. [[CrossRef](#)]
- Li, J.; Zhang, G. Dynamic surface control for path following of the USV-UAV with time-varying disturbances. In Proceedings of the 2022 34th Chinese Control and Decision Conference (CCDC), Hefei, China, 15–17 August 2022; pp. 3115–3120.
- Ccari, L.F.C.; Yanyachi, P.R. A Novel Neural Network-Based Robust Adaptive Formation Control for Cooperative Transport of a Payload Using Two Underactuated Quadcopters. *IEEE Access* **2023**, *11*, 36015–36028. [[CrossRef](#)]
- Fridman, E. Near-optimal H-infinity control of linear singularly perturbed systems. *IEEE Trans. Autom. Control* **1996**, *41*, 236–240. [[CrossRef](#)]
- Lu, G.P.; Yeung, L.E. H_∞ -control problem for linear systems with multiple time-delays via dynamic output feedback. *Math. Comput. Simul.* **2002**, *60*, 335–345. [[CrossRef](#)]
- Sun, L.Y.; Tong, S.C.; Liu, Y. Adaptive Backstepping Sliding Mode H_∞ Control of Static Var Compensator. *IEEE Trans. Control Syst. Technol.* **2011**, *19*, 1178–1185. [[CrossRef](#)]
- Dai, Y.; Wang, D.; Shen, F.Y.; Iqbal, J. A robust optimal control by grey wolf optimizer for underwater vehicle-manipulator system. *PLoS ONE* **2023**, *18*, e0287405. [[CrossRef](#)] [[PubMed](#)]
- Garcia, G.A.; Keshmiri, S.; Shukla, D. Nonlinear Control based on H-Infinity Theory for Autonomous Aerial Vehicle. In Proceedings of the 2017 International Conference on Unmanned Aircraft Systems (ICUAS'17), Miami, FL, USA, 13–16 June 2017; pp. 336–345.
- Rigatos, G.; Abbaszadeh, M. Nonlinear optimal control for multi-DOF robotic manipulators with flexible joints. *Optim. Control Appl. Methods* **2021**, *42*, 1708–1733. [[CrossRef](#)]
- Polyak, B.T.; Nazin, A.V.; Khlebnikov, M.V.; Nazin, S.A. Rejection of bounded disturbances via invariant ellipsoids technique. In Proceedings of the 45th IEEE Conference on Decision and Control, San Diego, CA, USA, 13–15 December 2006; pp. 1429–1434.
- Khlebnikov, M.V.; Polyak, B.T.; Kuntsevich, V.M. Optimization of linear systems subject to bounded exogenous disturbances: The invariant ellipsoid technique. *Autom. Remote Control* **2011**, *72*, 2227–2275. [[CrossRef](#)]
- Polyakov, A.; Poznyak, A. Invariant ellipsoid method for minimization of unmatched disturbances effects in sliding mode control. *Automatica* **2011**, *47*, 1450–1454. [[CrossRef](#)]

22. Gonzalez-Garcia, S.; Polyakov, A.E.; Poznyak, A.S. Using the method of invariant ellipsoids for linear robust output stabilization of spacecraft. *Autom. Remote Control* **2011**, *72*, 540–555. [[CrossRef](#)]
23. Gritli, H.; Belghith, S. LMI-based synthesis of a robust saturated controller for an underactuated mechanical system subject to motion constraints. *Eur. J. Control* **2021**, *57*, 179–193. [[CrossRef](#)]
24. Baleanu, D.; Hasanabadi, M.; Vaziri, A.M.; Jajarmi, A. A new intervention strategy for an HIV/AIDS transmission by a general fractional modeling and an optimal control approach. *Chaos Solitons Fractals* **2023**, *167*, 113078. [[CrossRef](#)]
25. Sereshki, Z.T.; Talebi, H.; Abdollahi, F. A nonlinear adaptive H_∞ optimal control method without solving HJIE: An analytical approach. *IEEE Trans. Autom. Control* **2024**. [[CrossRef](#)]
26. Ballesteros, M.; Fuentes-Aguilar, R.Q.; Chairez, I. Exponential Continuous Non-Parametric Neural Identifier with Predefined Convergence Velocity. *IEEE-CAA J. Autom. Sin.* **2022**, *9*, 1049–1060. [[CrossRef](#)]
27. Su, H.G.; Zhang, H.G.; Gao, D.W.Z.; Luo, Y.H. Adaptive Dynamics Programming for H_∞ Control of Continuous-Time Unknown Nonlinear Systems via Generalized Fuzzy Hyperbolic Models. *IEEE Trans. Syst. Man Cybern.-Syst.* **2020**, *50*, 3996–4008. [[CrossRef](#)]
28. Rigatos, G.; Busawon, K.; Abbaszadeh, M. A nonlinear optimal control approach for the truck and N-trailer robotic system. *IFAC J. Syst. Control* **2022**, *20*, 100191. [[CrossRef](#)]
29. Wang, Y.S.; Piao, M.N.; Chen, Z.Q.; Sun, M.W.; Sun, Q.L. Capability Exploration of Extended-State Observer-Based Control Under the Uncertain Case of Disturbance and Actuator Saturation. *IEEE Trans. Ind. Electron.* **2023**, *70*, 1841–1851. [[CrossRef](#)]
30. Altan, A.; Aslan, O.; Hacıoglu, R. Real-Time Control based on NARX Neural Network of Hexarotor UAV with Load Transporting System for Path Tracking. In Proceedings of the 2018 6th International Conference on Control Engineering & Information Technology (CEIT), Istanbul, Turkey, 25–27 October 2018.
31. Li, Z.J.; Su, C.Y.; Li, G.L.; Su, H. Fuzzy Approximation-Based Adaptive Backstepping Control of an Exoskeleton for Human Upper Limbs. *IEEE Trans. Fuzzy Syst.* **2015**, *23*, 555–566. [[CrossRef](#)]
32. Yu, J.P.; Shi, P.; Dong, W.J.; Chen, B.; Lin, C. Neural Network-Based Adaptive Dynamic Surface Control for Permanent Magnet Synchronous Motors. *IEEE Trans. Neural Netw. Learn. Syst.* **2015**, *26*, 640–645. [[CrossRef](#)]
33. Tong, S.C.; Sui, S.; Li, Y.M. Fuzzy Adaptive Output Feedback Control of MIMO Nonlinear Systems with Partial Tracking Errors Constrained. *IEEE Trans. Fuzzy Syst.* **2015**, *23*, 729–742. [[CrossRef](#)]
34. Li, Z.J.; Su, C.Y.; Wang, L.Y.; Chen, Z.T.; Chai, T.Y. Nonlinear Disturbance Observer-Based Control Design for a Robotic Exoskeleton Incorporating Fuzzy Approximation. *IEEE Trans. Ind. Electron.* **2015**, *62*, 5763–5775. [[CrossRef](#)]
35. Zhou, Q.; Shi, P.; Liu, H.H.; Xu, S.Y. Neural-Network-Based Decentralized Adaptive Output-Feedback Control for Large-Scale Stochastic Nonlinear Systems. *IEEE Trans. Syst. Man Cybern. Part B-Cybern.* **2012**, *42*, 1608–1619. [[CrossRef](#)]
36. Krstic, M.; Kokotovic, P.V.; Kanellakopoulos, I. *Nonlinear and Adaptive Control Design*; John Wiley & Sons, Inc.: Hoboken, NJ, USA, 1995.
37. Ma, J.J.; Zheng, Z.Q.; Li, P. Adaptive Dynamic Surface Control of a Class of Nonlinear Systems with Unknown Direction Control Gains and Input Saturation. *IEEE Trans. Cybern.* **2015**, *45*, 728–741. [[CrossRef](#)] [[PubMed](#)]
38. Chen, C.; Xie, L.H.; Xie, K.; Lewis, F.L.; Xie, S.L. Adaptive optimal output tracking of continuous-time systems via output-feedback-based reinforcement learning. *Automatica* **2022**, *146*, 110581. [[CrossRef](#)]
39. Won, D.; Kim, W.; Shin, D.; Chung, C.C. High-gain disturbance observer-based backstepping control with output tracking error constraint for electro-hydraulic systems. *IEEE Trans. Control Syst. Technol.* **2014**, *23*, 787–795. [[CrossRef](#)]
40. Khalil, H.K. High-gain observers in nonlinear feedback control. In *New Directions in Nonlinear Observer Design*; Springer: London, UK, 2007; pp. 249–268.
41. Adil, A.; N'Doye, I.; Laleg-Kirati, T.M. High-Gain Observer Design for Nonlinear Systems with Delayed Output Measurements using Time-Varying Gains. In Proceedings of the 2022 IEEE 61st Conference on Decision and Control (CDC), Cancún, Mexico, 6–9 December 2022; pp. 235–240.
42. Jaber, L.; Ichalal, D.; Oufroukh, N.A.; Nouvelière, L.; Mammar, S. A New High Gain Observer Based on Artificial Delays. In Proceedings of the 2023 IEEE International Conference on Networking, Sensing and Control (ICNSC), Marseille, France, 25–27 October 2023; pp. 1–6.
43. Vaidyanathan, S.; Lien, C.-H. *Applications of Sliding Mode Control in Science and Engineering*; Springer: Cham, Switzerland, 2017; Volume 709.
44. Cheng, X.; Liu, H.S.; Lu, W.K. Chattering-Suppressed Sliding Mode Control for Flexible-Joint Robot Manipulators. *Actuators* **2021**, *10*, 288. [[CrossRef](#)]
45. Fateh, A.; Momeni, H.; Masouleh, M.T. Taylor-based adaptive sliding mode control method for robot manipulators. *IET Control Theory Appl.* **2023**, *17*, 1105–1115. [[CrossRef](#)]
46. Miranda-Colorado, R. Finite-time sliding mode controller for perturbed second-order systems. *ISA Trans.* **2019**, *95*, 82–92. [[CrossRef](#)] [[PubMed](#)]
47. Gonzalezvelasco, E.A. Connections in Mathematical Analysis—The Case of Fourier-Series. *Am. Math. Mon.* **1992**, *99*, 427–441. [[CrossRef](#)]
48. Polycarpou, M.M.; Ioannou, P.A. A robust adaptive nonlinear control design. *Automatica* **1996**, *32*, 423–427. [[CrossRef](#)]
49. Zhao, Z.J.; Liu, Z.J.; He, W.; Hong, K.S.; Li, H.X. Boundary adaptive fault-tolerant control for a flexible Timoshenko arm with backlash-like hysteresis. *Automatica* **2021**, *130*, 109690. [[CrossRef](#)]

50. Ma, Y.H.; He, X.Y.; Zhang, S.; Sun, Y.B.; Fu, Q. Adaptive Compensation for Infinite Number of Actuator Faults and Time-Varying Delay of a Flexible Manipulator System. *IEEE Trans. Ind. Electron.* **2022**, *69*, 13141–13150. [[CrossRef](#)]
51. Lee, M.J.; Choi, Y.K. An adaptive neurocontroller using RBFN for robot manipulators. *IEEE Trans. Ind. Electron.* **2004**, *51*, 711–717. [[CrossRef](#)]
52. Spong, M.W. Modeling and Control of Elastic Joint Robots. *J. Dyn. Syst. Meas. Control.-Trans. ASME* **1987**, *109*, 310–319. [[CrossRef](#)]

Disclaimer/Publisher’s Note: The statements, opinions and data contained in all publications are solely those of the individual author(s) and contributor(s) and not of MDPI and/or the editor(s). MDPI and/or the editor(s) disclaim responsibility for any injury to people or property resulting from any ideas, methods, instructions or products referred to in the content.